Journal of Photochemistry and Photobiology B: Biology 116 (2012) 13–21

Contents lists available at SciVerse ScienceDirect

Journal of Photochemistry and Photobiology B: Biology

journal homepage: www.elsevier.com/locate/jphotobiol

A seven-coordinated manganese(II) complex with V-shaped ligand bis(*N*-benzylbenzimidazol-2-ylmethyl)benzylamine: Synthesis, structure, DNA-binding properties and antioxidant activities

Huilu Wu *, Jingkun Yuan, Ying Bai, Hua Wang, Guolong Pan, Jin Kong

School of Chemical and Biological Engineering, Lanzhou Jiaotong University, Lanzhou 730070, PR China

ARTICLE INFO

Article history:
Received 14 May 2012
Received in revised form 30 June 2012
Accepted 16 July 2012
Available online 26 July 2012

Keywords:
Benzimidazole
Manganese(II) complex
Crystal structure
DNA-binding property
Antioxidant property

ABSTRACT

A manganese(II) complex of the type, [Mn**L**(pic)$_2$]·H_2O, was obtained by the reaction of the V-shaped ligand bis(*N*-benzylbenzimidazol-2-ylmethyl)benzylamine (**L**) with Mn(pic)$_2$ (pic = picrate). The ligand **L** and Mn(II) complex were confirmed on the basis of elemental analysis, molar conductivities, ^{1}H NMR, IR, UV–vis spectra and X-ray crystallography. Single-crystal X-ray revealed that central Mn(II) atom is seven-coordinate with a MnN_3O_4 environment, in which ligand **L** acts as a tridentate N-donor. The remaining coordination sites were occupied by four O atoms afforded by two picrate anion. Interaction of the free ligand **L** and Mn(II) complex with DNA were investigated by spectrophotometric methods and viscosity measurements. The results suggested that both ligand **L** and Mn(II) complex bind to DNA in an intercalative binding mode, and DNA-binding affinity of the Mn(II) complex is stronger than that of ligand **L**. Moreover, antioxidant assay *in vitro* shows the Mn(II) complex possesses significant antioxidant activities.

1. Introduction

Benzimidazole and its derivatives have attracted considerable interests in recent years for their versatile properties in chemistry and pharmacology [1,2]. As a part of the chemical structure of vitamin B_{12} [3], the benzimidazole scaffold is a privileged structural motif for displaying chemical functionality in biologically active molecules [4]. Some of its derivatives have potent pharmacological applications as anticancer [5], antihypertensive [6], antiviral [7], anti-inflammatory [8], vasodilator [9] and antimicrobial agents [10]. Moreover, as a typical heterocyclic ligand, the large benzimidazole rings not only can provide potential supramolecular recognition sites for $\pi\cdots\pi$ stacking interactions, but also act as hydrogen bond acceptors and donors to assemble multiple coordination geometry [11].

The interaction of small molecules with DNA is a dynamic, thriving field which has drawn ever increasing research interests in recent decades [12–14]. An understanding that how these small molecules bind to DNA will potentially be useful in the design of such new compounds, which can recognize specific sites or conformations of DNA [15–17]. Hence, studies on the interaction of small molecules, such as transition metal complexes, with DNA have been a pet subject for the researchers in the field of bioinorganic chemistry [18]. Due to their intriguing variety architectures [19,20] and important properties that span from luminescence [21] to biological activities [22], the rational design and synthesis of the transition metal complexes containing benzimidazole-based ligands also gives the possibility for further research, such as design of structural probes and the development of novel therapeutics.

As a section of our program for constructing of V-shaped bisbenzimidazol ligands containing the different substitutive groups with corresponding transition metal complexes, we have investigated the DNA binding ability of such complexes in our previous publications [23–26]. In this contribution, the synthesis, characterization and DNA-binding activities of Mn(II) complex with a V-shaped ligand are presented. Additionally, the antioxidant property for Mn(II) complex have also been presented and discussed in detail.

2. Experimental section

2.1. Materials and methods

Calf thymus DNA (CT-DNA), ethidium bromide (EB), nitroblue tetrazolium nitrate (NBT), methionine (MET) and riboflavin ($VitB_2$) were obtained from Sigma–Aldrich Co. (USA). EDTA and safranin were produced in China. Other reagents and solvents were reagent grade obtained from commercial sources and used without further purification. Tris-HCl buffer, Na_2HPO_4–NaH_2PO_4 buffer, and

* Corresponding author. Tel.: +86 13893117544.
E-mail address: wuhuilu@163.com (H. Wu).

1011-1344/$ - see front matter © 2012 Elsevier B.V. All rights reserved.
http://dx.doi.org/10.1016/j.jphotobiol.2012.07.005

EDTA–Fe(II) solution were prepared using bi-distilled water. The solution of CT-DNA gave a ratio of UV absorbance at 260 and 280 nm, A_{260}/A_{280}, of 1.8–1.9, indicating that the DNA was sufficiently free of protein [27]. The stock solution of DNA (2.5×10^{-3} M) was prepared in 5 mM Tris-HCl/50 mM NaCl buffer (pH = 7.2, stored at 4 °C and used when not more than 4 days). The DNA concentration was determined by measuring the UV absorption at 260 nm, taking the molar absorption coefficient (ε_{260}) of CT-DNA as 6600 M^{-1} cm^{-1} [28]. $Mn(pic)_2$ was obtained by the reaction of the picric acid with $MnCO_3$. The stock solution of **L** and Mn(II) complex were dissolved in DMF at the concentration 3×10^{-3} M.

Elemental analyses were determined using a Carlo Erba 1106 elemental analyzer. Electrolytic conductance measurements were made with a DDS-307 type conductivity bridge using 3×10^{-3} mol L^{-1} solutions in DMF at room temperature. The IR spectra were recorded in the 4000–400 cm^{-1} region with a Nicolet FT-VERTEX 70 spectrometer using KBr pellets. Electronic spectra were taken on a Lab-Tech UV Bluestar spectrophotometer. The fluorescence spectra were performed on a LS-45 spectrofluorophotometer. The absorbance was measured with Spectrumlab 722sp spectrophotometer at room temperature. ^{1}H NMR spectra were recorded on a Varian VR300-MHz spectrometer with TMS as an internal standard.

2.2. Synthesis

2.2.1. Synthesis of the ligand *L*

The precursor bis(2-benzimidazol-2-ylmethyl)benzylamine (bbb) was synthesized following a slight modification of the procedure in ref [29]. bbb (7.34 g, 20 mmol) and potassium (1.56 g, 40 mmol) were put in tetrahydrofuran (150 mL), the solution was refluxed on a water bath for 5 h with stirring. Then, benzylbromide (6.84 g, 40 mmol) was added to this solution. With the dropping of benzylbromide, the solution gradually becomes cream yellow. After that, the resulting solution was concentrated and cooled, a pale yellow solid separating out and the pale yellow precipitate was filtered, washed with massive water, and recrystallized from ethanol to give the ligand.

Yield: 5.56 g, 61%; m.p.: 156–158 °C. Found (%): C, 81.02; H, 6.26; N, 12.69. Calcd. (%) for $C_{37}H_{33}N_5$: C, 81.14; H, 6.07; N, 12,79. ^{1}H NMR (DMSO-d_6 400 MHz) δ/ppm: 3.77 (m, 2H, —CH_2—Ar), 3.85 (s, 4H, —CH_2-benzimidazol), 5.27 (m, 4H, —CH_2—Ar), 6.89 (m, 5H, *H*-benzene ring), 7.19–7.26 (s, 10H, H-benzene ring), 7.42–7.64 (m, 8H, *H*-benzimidazol ring). Λ_m(DMF, 297 K): 4.16 S cm^2 mol^{-1}. UV–vis (λ, nm): 279, 286. FT–IR (KBr ν/cm^{-1}): 740, ν(*o*–Ar); 1286, ν(C—N); 1464, ν(C=N), 1612, ν(C=C).

The synthetic routine of ligand **L** is showed in Scheme 1.

2.2.2. Synthesis of complex: $[Mn\mathbf{L}(pic)_2]\cdot H_2O$

To a stirred solution of **L** (273.5 mg, 0.50 mmol) in hot EtOH (10 mL) was added $Mn(pic)_2$ (127.8 mg, 0.25 mmol) in EtOH (2 mL). A yellow crystalline product formed rapidly. The precipitate was filtered off, washed with EtOH and absolute Et_2O, and dried in *vacuo*. The dried precipitate was dissolved in MeCN to form a yellow solution into which Et_2O was allowed to diffuse at room temperature. Crystal suitable for X-ray measurement was obtained after 3 weeks.

Yield: 246.5 mg (68%). Found (%): C, 54.48; H, 3.87; N, 14.47. Calcd. (%) for $C_{49}H_{39}MnN_{11}O_{15}$: C, 54.65; H, 3.65; N, 14.31. Λ_m(DMF, 297 K): 39.38 S cm^2 mol^{-1}. UV–vis (λ, nm): 270, 279, 381. FT–IR (KBr ν/cm^{-1}): 746, ν (*o*–Ar); 1267, ν(C—N); 1365, ν(O—N—O); 1490, ν(C=N); 1618, ν(C=C).

2.3. X-ray crystallography

A suitable single crystal was mounted on a glass fiber, and the intensity data were collected on a Bruker Smart CCD diffractometer with graphite-monochromated Mo Kα radiation (λ = 0.71073 Å) at 296 K. Data reduction and cell refinement were performed using the SMART and SAINT programs [30]. The structure was solved by direct methods and refined by full-matrix least-squares against F^2 of data using SHELXTL software [31]. All H atoms were found in difference electron maps and subsequently refined in a riding-model approximation with C—H distances ranging from 0.93 to 0.97 Å and $U_{iso}(H) = 1.2\ U_{eq}(C)$.

2.4. DNA-binding experiments

2.4.1. Viscosity titration measurements

Viscosity experiments were conducted on an Ubbelodhe viscometer, immersed in a water bath maintained at 25.0 ± 0.1 °C. The flow time was measured with a digital stopwatch and each sample was tested, three times to get an average calculated time. Titrations were performed for the complexes (3–30 μM), and each compound was introduced into CT-DNA solution (42.5 μM) present in the viscometer. Data were analysed as $(\eta/\eta_0)^{1/3}$ versus the ratio of the concentration of the compound to CT-DNA, where η is the viscosity of CT-DNA in the presence of the compound and η_0 is the viscosity of CT-DNA alone. Viscosity values were calculated from the observed flow time of CT-DNA-containing solutions corrected from the flow time of buffer alone (t_0), $\eta = (t - t_0)$ [32].

2.4.2. Electronic absorption titration

All spectrophotometric measurements were performed in thermostated quartz sample cells at 25 °C. Solutions for analysis were prepared by dilution of stock solutions immediately before the experiments. Spectrophotometer slit widths were kept at 1 nm for absorption spectroscopy and 5/5 nm for emission spectroscopy. Electronic absorption titration experiments were performed by maintaining the concentration of the test compounds (ligands/complexes) as constant (30 μM) while gradually increasing the concentration of CT-DNA. To obtain the absorption spectra, the required amount of CT-DNA was added to both the compound and reference solutions, in order to eliminate the absorbance of CT-DNA itself. Each sample solution was scanned in the range of 190–500 nm, and the mixture was allowed to equilibrate for 5 min before the spectra were recorded. From the absorption titration data, the binding constant (K_b) was determined using the equation [33]:

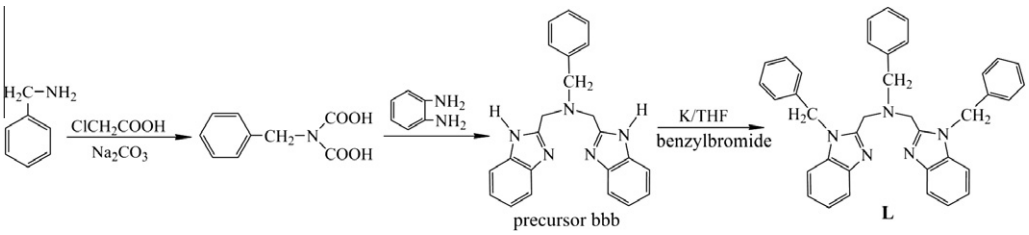

Scheme 1. Synthetic routine of ligand **L**.

Table 1
Crystal data and structure refinement for $[Mn\mathbf{L}(pic)_2]\cdot H_2O$.

Complex	$[Mn\mathbf{L}(pic)_2]\cdot H_2O$
Molecular formula	$C_{49}H_{39}MnN_{11}O_{15}$
Molecular weight	1076.85
Color	yellow
Crystal size (mm^3)	$0.32 \times 0.28 \times 0.26$
Crystal system	Triclinic
Space group	*P-1*
a (Å)	10.6596(15)
b (Å)	12.9361(18)
c (Å)	18.509(3)
α (°)	87.0440(10)
β (°)	81.6040(10)
γ (°)	77.5880(10)
V ($Å^3$)	2465.4(6)
Z	2
T (K)	296(2)
D_{calcd} (g cm^{-3})	1.451
F (000) (e)	1110
θ Range for data collection (°)	2.39–25.99
hkl range	$-12 \leqslant h \leqslant 13$, $-15 \leqslant k \leqslant 15$, $-22 \leqslant l \leqslant 22$
Reflections collected	18758
Independent reflections	9517 [R_{int} = 0.0253]
Refinement method	Full-matrix least-squares on F^2
Data/restraints/parameters	9517/17/685
Final R_1/wR_2 indices [$I \geqslant 2\sigma(I)$][a]	0.0495/0.1185
R_1/wR_2 indices (all data)[a]	0.0758/0.1358
Goodness-of-fit on F^2	1.015
Largest diff. peak and hole (e $Å^{-3}$)	0.647 and −0.394

$$[DNA]/(\varepsilon_a - \varepsilon_f) = [DNA]/(\varepsilon_b - \varepsilon_f) + 1/K_b(\varepsilon_b - \varepsilon_f)$$

where [DNA] is the concentration of CT-DNA in base pairs, ε_a corresponds to the observed extinction coefficient (Aobsd/[M]), ε_f corresponds to the extinction coefficient of the free compound, ε_b is the extinction coefficient of the compound when fully bound to CT-DNA, and K_b is the intrinsic binding constant. The ratio of slope to intercept in the plot of $[DNA]/(\varepsilon_a - \varepsilon_f)$ versus [DNA] gave the value of K_b.

2.4.3. Competitive binding with ethidium bromide

The enhanced fluorescence of EB in the presence of DNA can be quenched by the addition of a second molecule [34,35]. The extent of fluorescence quenching of EB bound to CT-DNA can be used to determine the extent of binding between the second molecule and CT-DNA. Competitive binding experiments were carried out in the buffer by keeping [DNA]/[EB] = 1 and varying the concentrations of the compounds. The fluorescence spectra of EB were measured using an excitation wavelength of 520 nm, and the emission range was set between 550 and 750 nm. The influence of the addition of each compound to the DNA-EB complex solution has been obtained by recording the variation of the fluorescence emission spectra. The spectra were analyzed according to the classical Stern–Volmer equation [36]:

$$I_0/I = 1 + K_{SV}$$

where I_0 and I are the fluorescence intensities at 599 nm in the absence and presence of the quencher, respectively, *K*sv is the linear Stern–Volmer quenching constant, and [*Q*] is the concentration of the quencher. In these experiments [CT-DNA] = 2.5×10^{-3} mol L^{-1}, [EB] = 2.2×10^{-3} mol L^{-1}.

2.5. Antioxidant property

2.5.1. Hydroxyl radical scavenging activity

Hydroxyl radicals were generated in aqueous media through the Fenton-type reaction [37,38]. The aliquots of reaction mixture (3 mL) contained 1.0 mL of 0.10 mmol aqueous safranin, 1 mL of 1.0 mmol aqueous EDTA–Fe(II), 1 mL of 3% aqueous H_2O_2, and a series of quantitative microadditions of solutions of the test compound. A sample without the tested compound was used as the control. The reaction mixtures were incubated at 37 °C for 30 min in a water bath. The absorbance was then measured at 520 nm. All the tests were run in triplicate and are expressed as the mean and standard deviation (SD) [39]. The scavenging effect for OH· was calculated from the following expression:

$$\text{Scavenging ratio}(\%) = [(A_i - A_0)/(A_c - A_0)] \times 100\%$$

where A_i = absorbance in the presence of the test compound; A_0 = absorbance of the blank in the absence of the test compound; A_c = absorbance in the absence of the test compound, EDTA-Fe(II) and H_2O_2.

2.5.2. Superoxide radical scavenging activity

The superoxide radical was investigated indirectly using the system of MET-VitB_2-NBT [40,41]. The aqueous solution contained 0.5 mL 3.3×10^{-5} M VitB_2, 1 mL 2.3×10^{-4} M NBT, 1 mL 0.05 M MET, and the complexes of various concentrations were prepared with 0.067 M phosphate buffer (Na_2HPO_4–NaH_2PO_4, pH = 7.8). They were illuminated by a fluorescent lamp with a constant light intensity at 25 °C. The optical absorbance (A) of the solution at 560 nm was measured with various illumination periods (t). All the tests were run in triplicate and are expressed as the mean and standard deviation (SD) [39]. The scavenging effect for $O_2^{-\cdot}$ was calculated from the following expression:

$$\text{Scavenging ratio}(\%) = [(A_0 - A_i)/A_0] \times 100\%$$

where A_i = absorbance in the presence of the tested compound, A_0 = absorbance in the absence of the tested compound.

3. Results and discussion

Caution: Picrate salts of metal complexes with organic ligands are potentially explosive. Only small amounts of the material should be prepared and handled with great care.

Ligand **L** and Mn(II) complex are very stable in the air. Mn(II) complex is remarkably soluble in polar aprotic solvents such as DMF, DMSO and MeCN; slightly soluble in ethanol, methanol, ethyl acetate and chloroform; insoluble in water, Et_2O, and petroleum ether. The molar conductivities in DMF solution indicate that ligand **L** and Mn(II) complex are nonelectrolyte compounds [42,43].

3.1. IR and electronic spectra

The IR spectra of the Mn(II) complex are closely related to that of the free ligand **L**. One of the most diagnostic changes occurs in

Table 2
Selected bond distances (Å) and angles (°).

Complex	$[Mn\mathbf{L}(pic)_2]\cdot H_2O$			
Bond distances	Mn—O(1)	2.151(2)	Mn—N(1)	2.502(2)
	Mn—O(2)	2.466(2)	Mn—N(3)	2.206(2)
	Mn—O(8)	2.080(2)	Mn—N(5)	2.221(2)
	Mn—O(9)	2.497(2)		
Bond angles	O(8)—Mn—O(1)	86.47(8)	N(3)—Mn—O(9)	136.42(8)
	O(8)—Mn—N(3)	93.64(8)	N(5)—Mn—O(9)	86.51(8)
	O(1)—Mn—N(3)	147.17(8)	O(2)—Mn—O(9)	143.92(7)
	O(8)—Mn—N(5)	157.08(8)	O(8)—Mn—N(1)	103.31(8)
	O(1)—Mn—N(5)	85.51(8)	O(1)—Mn—N(1)	139.43(8)
	N(3)—Mn—N(5)	104.64(8)	N(3)—Mn—N(1)	72.40(7)
	O(8)—Mn—O(2)	101.24(9)	N(5)—Mn—N(1)	70.19(7)
	O(1)—Mn—O(2)	70.10(7)	O(2)—Mn—N(1)	142.15(7)
	N(3)—Mn—O(2)	77.74(8)	O(9)—Mn—N(1)	72.33(7)
	N(5)—Mn—O(2)	96.13(8)	O(1)—Mn—O(9)	74.27(8)
	O(8)—Mn—O(9)	70.65(8)		

the region between 1650 and 1250 cm^{-1}. The spectra of **L** show a strong band at 1464 cm^{-1} and weak bands at 1612 cm^{-1}. By analogy with the assigned bands of imidazole, two bands are attributed to the ν(C=N) and ν(C=C) frequencies of the benzimidazole group, respectively [44–46]. The band ν(C=N) undergo a red shift (about 26 nm) in the Mn(II) complex as compared to free ligand **L**, which can be attributed to the coordination of the benzimidazole nitrogen to the metal center [47]. As found in other metal complexes with benzimidazoles, these are the preferred nitrogen atom for coordination [48]. Moreover, Information regarding the possible bonding modes of the picrate and benzimidazole rings may also be obtained from the IR spectra [24,25].

DMF solutions of ligand **L** and Mn(II) complex show, as expected, almost identical UV spectra. The UV bands of ligand **L** (286, 279 nm) are undergo a red-shifted about 9 nm for Mn(II) complex, which is evidence of C=N coordination to the metal center. These bands are assigned to $n \rightarrow \pi^*$ and $\pi \rightarrow \pi^*$ (imidazole) transitions. The picrate bands (observed at 381 nm) are assigned to $\pi \rightarrow \pi^*$ transitions [23,24].

3.2. X-ray structures of the complex

Basic crystal data, description of the diffraction experiment, and details of the structure refinement are given in Table 1. Selected bond distances and angles are presented in Table 2.

The crystal structure of Mn(II) complex consists of a discrete [Mn**L**$(pic)_2$] and a solvent water molecule. The solvent water molecules are present in the crystal lattice, but have no direct interactions with the [Mn**L**$(pic)_2$]. The ORTEP structure (30% probability ellipsoids) of the [Mn**L**$(pic)_2$] with atom-numberings is shown in Fig. 1.

The central Mn(II) atom is seven-coordinated with a MnN_3O_4 coordination environment. As depicted in the Fig. 2, the coordination geometry of the central Mn(II) atom is a distorted monocapped trigonal prismatic, made up by four O atoms provided by two picrate and three N atoms afforded by a tridentate ligand **L**. Three N atoms constructed an undersurface while another undersurface was constituted by three O atoms (O1, O2, O8) and the O9 atom in the capping position [49].

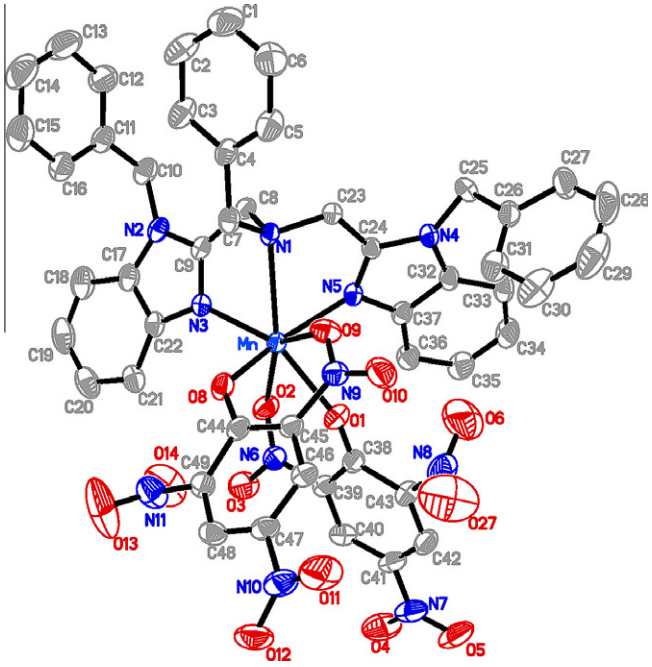

Fig. 1. Molecular structure and atom numberings of [Mn**L**$(pic)_2$] with hydrogen atoms were omitted for clarity.

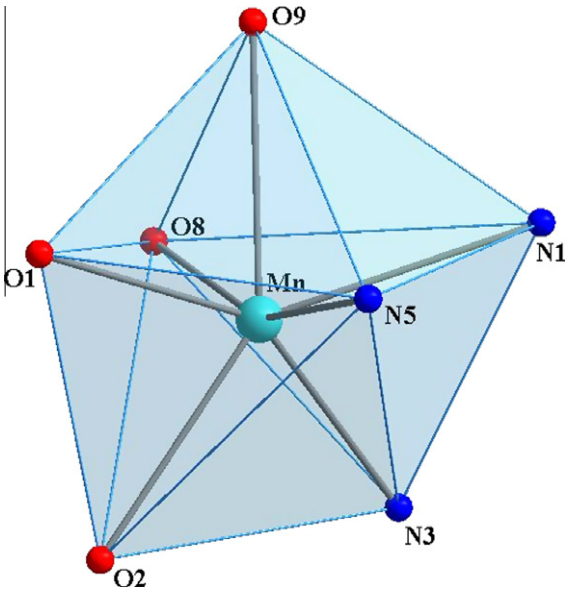

Fig. 2. The coordination sphere around the Mn(II) atom showing the monocapped (O9) trigonal prismaticin light blue.

As shown in Fig. 3, there are two types of the $\pi\cdots\pi$ interactions in Mn(II) complex [50–53]: (i) between benzene ring and picrate, d = 3.722 Å (d = centroid-to-centroid distance). (ii) between two benzimidazole rings from different structure units, d = 3.884 Å. Hence, an infinite 2-D (two dimension) layer is propagated due to the $\pi\cdots\pi$ interactions.

Due to the exist of the solvent water molecule which inlayed in the coordination cations as a sandwich, such arrangement not only can provide some groups for the formation of hydrogen bonds that make the crystal structure more stable, but also contribute to construct an infinite 3-D network (Fig. 4). The distinct topological structure affords an opportunity to investigate the potential in molecular recognition and gas absorption.

3.3. DNA binding properties

3.3.1. Viscosity titration measurements

Hydrodynamic measurements that are sensitive to the length change (i.e., viscosity and sedimentation) are regarded as the least ambiguous and the most critical tests of a interaction model in solution in the absence of crystallographic structural data [27,54]. A classical intercalative molecular interaction causes a significant increase in viscosity of the DNA solution due to the increase in separation of the base pairs at the intercalation sites and hence an increase in the overall DNA length [55,56]. Whereas, agents bound to DNA through groove binding do not alter the relative viscosity of DNA, and agents electrostatically bound to DNA will bend or kink the DNA helix, reducing its effective length and its viscosity, concomitantly [54,57].

Viscosity titration measurements were carried out to clarify the interaction modes between the investigated compounds and CT-DNA. The results of ligand **L** and Mn(II) complex on the viscosities of CT-DNA are shown in Fig. 5. The viscosity of CT-DNA is increasing steadily with the increment of ligand **L** and Mn(II) complex, indicating that ligand **L** and Mn(II) complex can interaction with CT-DNA in an intercalate mode, which may due to the large coplanar aromatic rings in two compounds that facilitate it intercalating to the base pairs of double helical DNA [55,56].

3.3.2. Absorption spectroscopic studies

The application of electronic absorption spectroscopy is one of the most useful techniques for DNA binding studies [33]. In

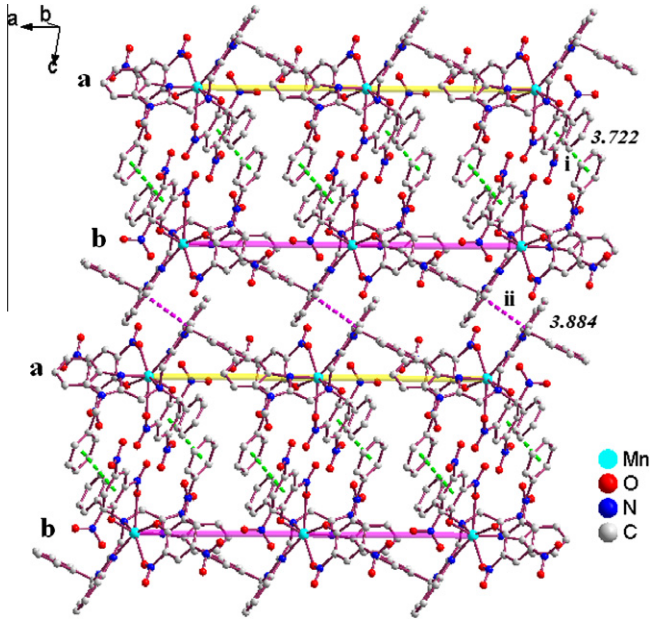

Fig. 3. 2-D layer formed *via* $\pi\cdots\pi$ interactions in [Mn**L**(pic)$_2$]·H$_2$O, hydrogen atoms and solvent molecules were omitted for clarity (different interactions are distinguished by different colors). (For interpretation of the references to color in this figure legend, the reader is referred to the web version of this article.)

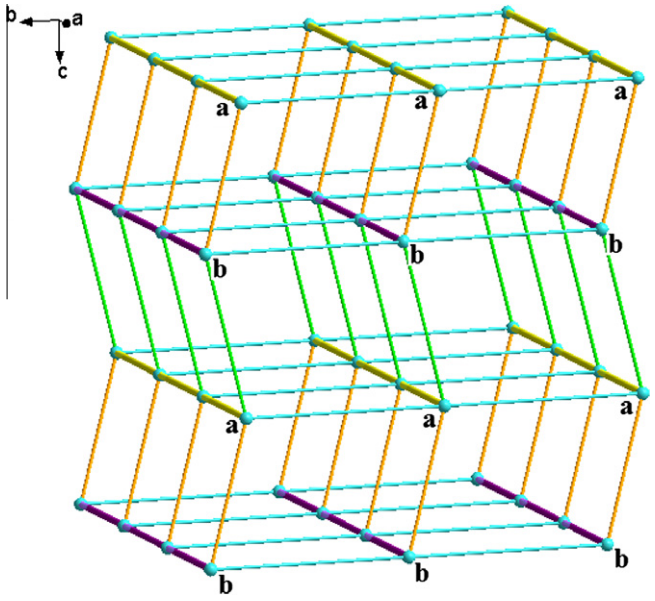

Fig. 4. 3-D network formed in [Mn**L**(pic)$_2$]·H$_2$O (In order to simplify, only central Mn(II) atoms were reserved).

general, compound binding with DNA through intercalation usually results in hypochromism and bathochromism, due to the intercalative mode involving a strong stacking interaction between an aromatic chromophore and the DNA base pairs. The extent of the hypochromism commonly parallels the intercalative binding strength [58]. The absorption spectra of ligand **L** and Mn(II) complex in the absence or presence of CT-DNA are given in Fig. 6. As the DNA concentration is increased, the hypochromism reaches as high as 28.32% at 272 nm for free ligand **L**; 44.39% at 271 nm for Mn(II) complex. The λ_{max} for ligand **L** and Mn(II) complex have a slight red shifts of about 1–2 nm under identical experimental conditions. The results suggested an association of the compound with DNA and it is also likely that ligand **L** and Mn(II) complex bind to the helix by intercalation, and it is noteworthy that the hypochromicity of Mn(II) complex is greater than that of ligand **L** [59,60].

To compare quantitatively the affinity of ligand **L** and Mn(II) complex towards DNA, the intrinsic binding constant (K_b) of ligand **L** and Mn(II) complex was calculated by plotting the changes in the absorbance of the complex upon incremental addition of increasing concentration of DNA. The K_b values of ligand **L** and Mn(II) complex are $1.78 \times 10^3\ M^{-1}$ ($R = 0.99$ for 16 points), $4.35 \times 10^4\ M^{-1}$ ($R = 0.99$ for 16 points), respectively. Therefore, compare with the classic DNA-intercalative reagent, such as Ethidium bromide (EB), acridine orange (AO), methylene blue (MB) [61], we speculate that ligand **L** and Mn(II) complex most possibly binds to DNA in an intercalation mode. The magnitude of K_b value is parallel to the intercalative strength and the affinity of a compound binding to DNA [59,60]. Hence, the result of the absorption spectral suggested that DNA-binding affinity of the Mn(II) complex is stronger than that of ligand **L,** which is consistent with the above viscosity titration measurements results.

3.3.3. Competitive binding with ethidium bromide

Ethidium bromide, a polycyclic aromatic dye, is the most widely used fluorescence probe for DNA structure. It binds to DNA by intercalation within the stacked bases [62]. It has been reported that the enhanced fluorescence of the EB–DNA complex can be quenched at least partially by the addition of a second molecule and this could be used to assess the relative affinity of the molecule for DNA [63]. No luminescence was observed for ligand **L** and Mn(II) complex at room temperature in any organic solvent or in the presence of CT-DNA. So the binding of complexes with CT-DNA cannot be directly presented in the emission spectra. Therefore, competitive EB binding studies could be undertaken in order to examine the binding of each complex with DNA.

The emission spectra of EB-DNA system in the absence and presence of complex are displayed in Fig. 7. The behaviors of ligand **L** and Mn(II) complex are in good agreement with the Stern–Volmer equation, which provide further evidence that there are some interactions between ligand **L** and Mn(II) complex and DNA. The K_{sv} values of ligand **L** and Mn(II) complex are $1.67 \times 10^4\ M^{-1}$ ($R = 0.98$ for 11 points in the linear part), $2.91 \times 10^4\ M^{-1}$ ($R = 0.97$ for 10 points in the linear part), respectively. The phenomena suggest that ligand **L** and Mn(II) complex can compete for DNA-binding sites with EB and displace it from the EB-DNA system [64], which is usually characteristic of the intercalative interaction of compounds with DNA [65]. Moreover, the affinity for DNA is more strongly in case of Mn(II) complex when compared with Ligand **L**. Such a trend is consistent with the previous viscosity titration and absorption spectral results.

Based on the results of viscosity measurements and spectrophotometric methods above, we found that the affinity for DNA is more strongly in case of Mn(II) complex when compared with the ligand **L**. For this difference, we attributed to three possible reasons. (i) By comparison of the molecular structure of the ligand **L** and Mn(II) complex, we find the greater number of coplanar aromatic rings may lead to higher affinity for DNA [25,26]. (ii) The charge transfer of coordinated ligands caused by the coordination of the central atom, lead to the decrease of the charge density of the plane conjugate system, which is conducive to insert [66]. (iii) This difference in their DNA binding ability also could be attributed to the presence of an electron deficient center in the charged Mn(II) complex where an additional interaction between the complex and phosphate rich DNA back bone may occur [67,68].

3.4. Antioxidant property

Since some similar complexes exhibit reasonable DNA-binding affinity, it is worthwhile considered to study other potential

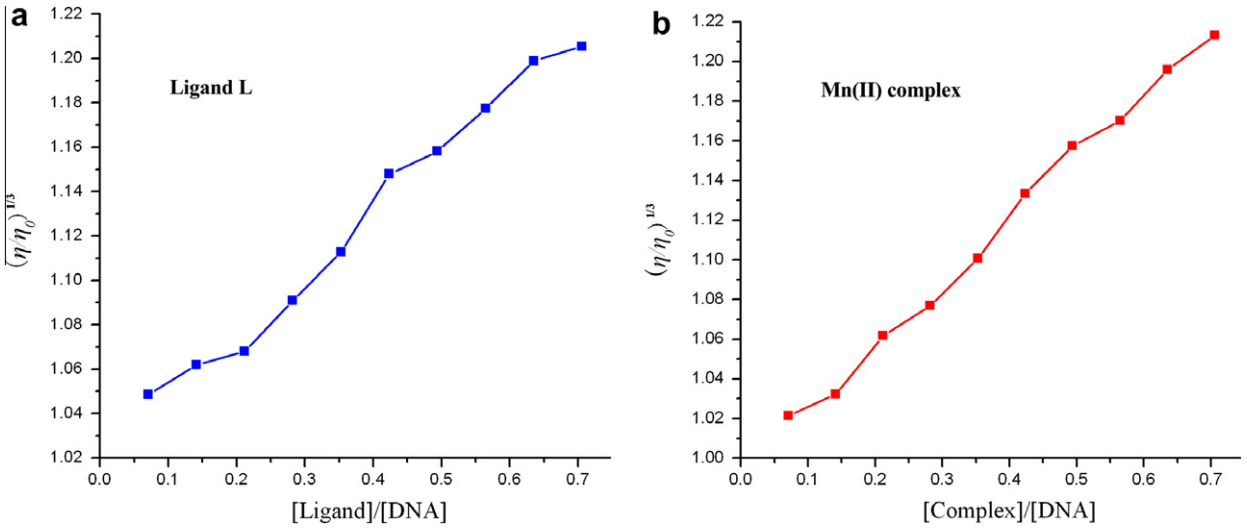

Fig. 5. Effect of increasing amounts of (a) ligand **L** and (b) Mn(II) complex on the relative viscosity of CT-DNA at 25.0 ± 0.1 °C.

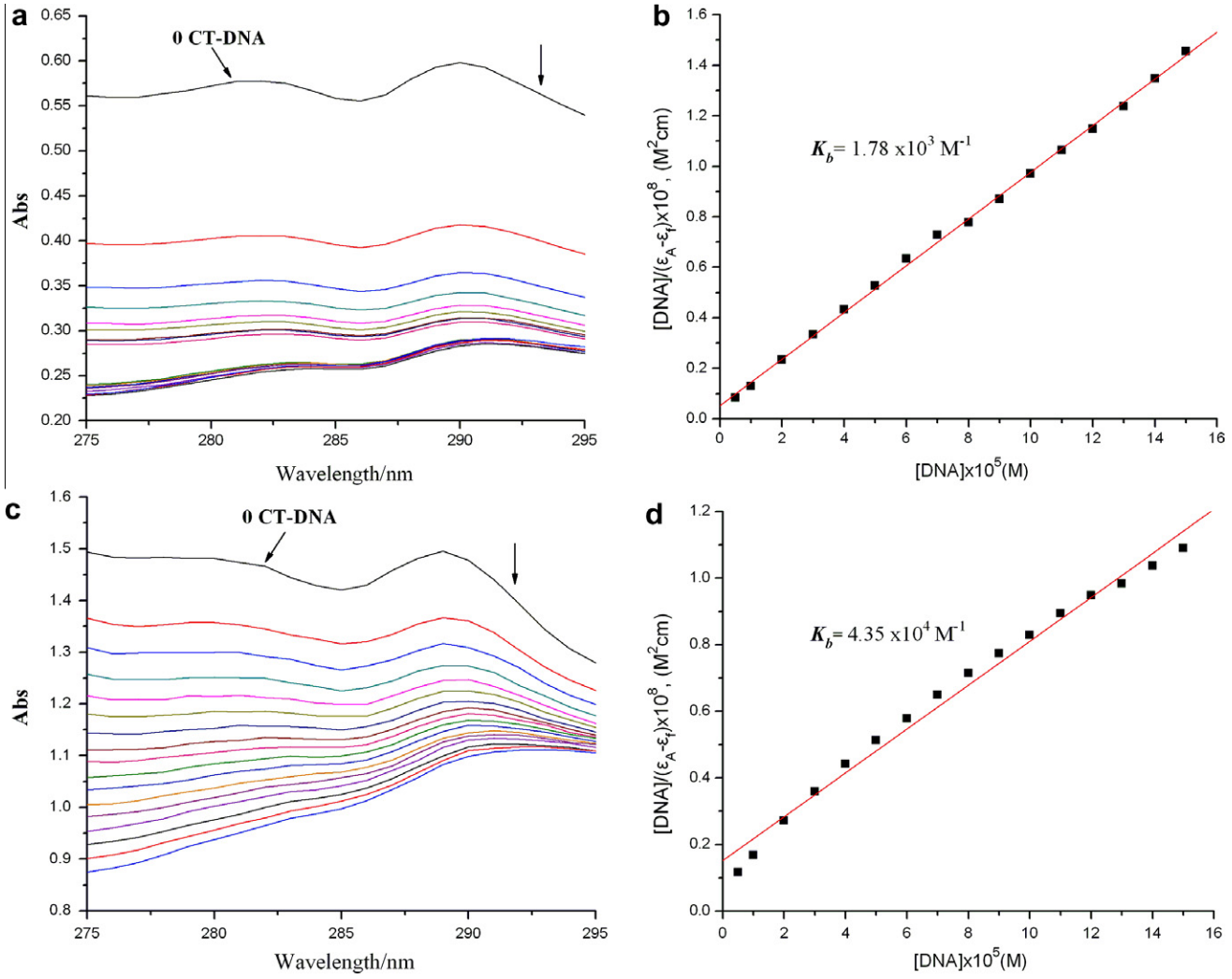

Fig. 6. Electronic spectra of (a) ligand **L**, (c) Mn(II) complex in Tris–HCl buffer upon addition of CT-DNA. [Compound] = 3 × 10^{-5} M^{-1}, [DNA] = 2.5 × 10^{-5} M^{-1}. Arrow shows the emission intensity changes upon increasing DNA concentration. Plots of [DNA]/($\varepsilon_a - \varepsilon_f$) versus. [DNA] for the titration of (b) ligand **L**, (d) Mn(II) complex with CT-DNA.

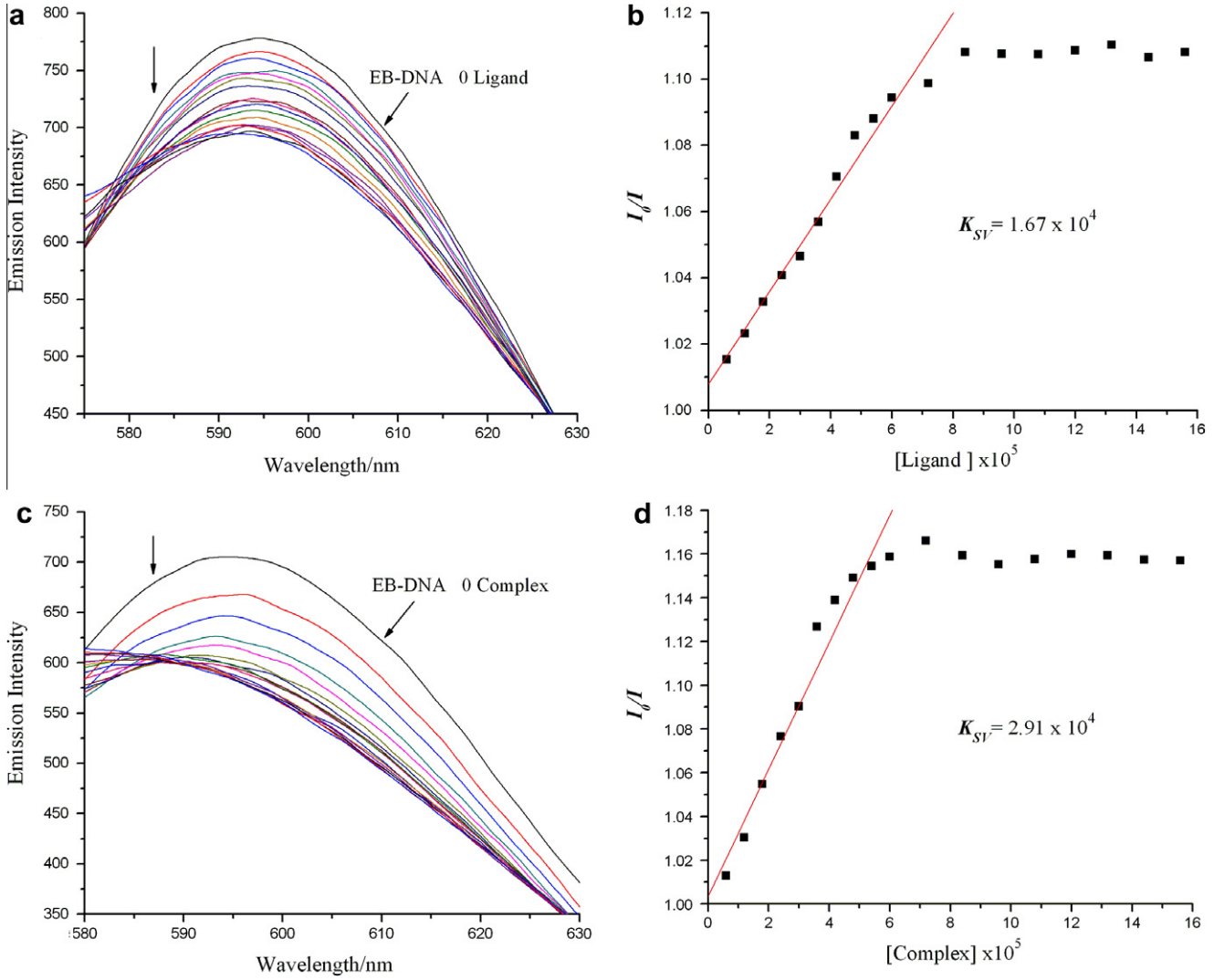

Fig. 7. Emission spectra of EB bound to CT-DNA in the presence of (a) ligand **L** and (c) Mn(II) complex; [Compound] = 3×10^{-5} M; λ_{ex} = 520 nm. The arrows show the intensity changes upon increasing concentrations of the complexes. Fluorescence quenching curves of EB bound to CT-DNA by (b) ligand **L** and (d) Mn(II) complex. (Plots of I_0/I versus [Complex]).

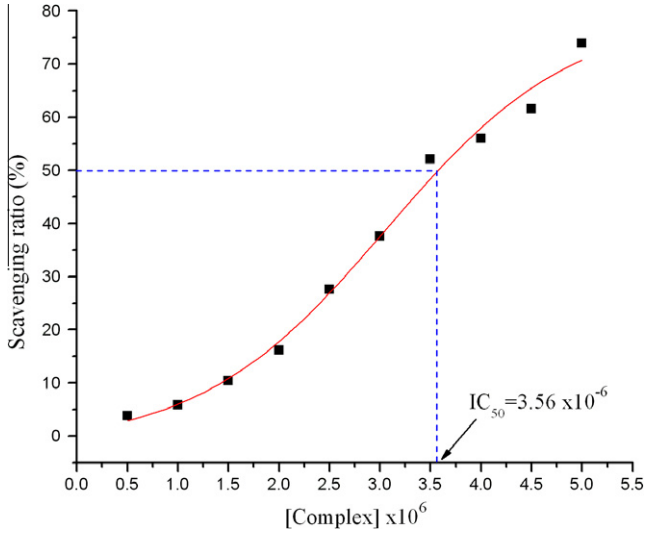

Fig. 8. A plot of scavenging percentage (%) versus concentration of the Mn(II) complex on hydroxyl radical.

aspects, such as antioxidant and antiradical activity. It is a well-documented fact that some transition metal complexes display significant antioxidant activity [69–71] and therefore we undertook a systematic investigation on the antioxidant potential of free ligand **L** and Mn(II) complex .

3.4.1. Hydroxyl radical scavenging activity

We compared the ability of Mn(II) complex to scavenge hydroxyl radicals with those of the well-known natural antioxidants mannitol and vitamin C, using the same method as reported in a previous paper [72]. The 50% inhibitory concentration (IC_{50}) value of mannitol and vitamin C are about 9.6×10^{-3} and 8.7×10^{-3} M^{-1}, respectively. As shown in Fig. 8, according to the antioxidant experiments, the IC_{50} values of Mn(II) complex is 3.56×10^{-6} M^{-1}, which implies that Mn(II) complex has the preferable ability to scavenge hydroxyl radical. It can be concluded that a much less or no scavenging activity was exhibited by the free ligand **L** when compared to that of Mn(II) complex which may be due to the chelation of ligand with the central metal atom [73]. The lower IC_{50} values observed in antioxidant assays demonstrate that Mn(II) complex has a strong potential to be applied as scavengers to eliminate the radicals.

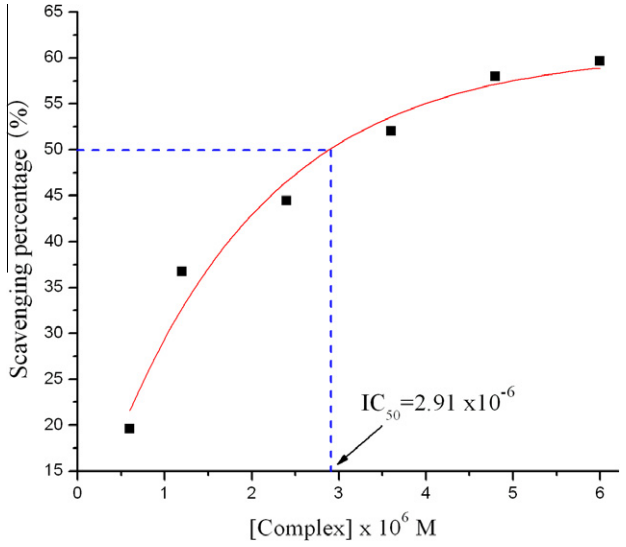

Fig. 9. A plot of scavenging percentage (%) versus concentration of the Mn(II) complex on superoxide radical.

3.4.2. Superoxide radical scavenging activity

SOD activity was monitored by reduction of nitro blue tetrazolium (NBT) with $O_2^{-\cdot}$ generated by xanthine/xanthine oxidase system. As the reaction proceeds, the Farmazan color is developed and the color change from colorless to blue appeared which was associated with an increase in the absorbance at 560 nm. The ligand **L** does not show significant activity against the same radical under identical experimental conditions compared with Mn(II) complex. As can be seen from Fig. 9, Mn(II) complex shows an IC_{50} value of 2.91×10^{-6} M^{-1}, which indicates that it has potent scavenging activity for superoxide radical ($O_2^{-\cdot}$). The results indicate that Mn(II) complex exhibits a fine superoxide radical scavenging activity and may be acted as an inhibitor (or a drug) to scavenge superoxide radical ($O_2^{-\cdot}$) *in vivo* which need further investigation.

4. Conclusion

In this work, ligand bis(*N*-allylbenzimidazol-2-ylmethyl)benzylamine and its Mn(II) complex have been synthesized and characterized. The crystal structure of $[Mn\mathbf{L}(pic)_2]\cdot H_2O$ is seven-coordinated adopting a distorted monocapped trigonal prismatic. The DNA-binding experimental results suggest that ligand **L** and Mn(II) complex bind to DNA in an intercalation mode, and the affinity of Mn(II) complex is stronger than that of ligand **L**, which are due to the large coplanar aromatic rings in two compounds that facilitate them intercalating to the base pairs of double helical DNA. Furthermore, the Mn(II) complex has stronger ability of antioxidation for hydroxyl radical and superoxide radical. These findings indicate that ligand **L** and Mn(II) complex have many potential practical applications for the development of nucleic acid molecular probes and new therapeutic reagents for diseases on the molecular level and warrant further *in vivo* experiments and pharmacological assays.

Acknowledgements

The authors acknowledge the financial support and Grant from 'Qing Lan' Talent Engineering Funds by Lanzhou Jiaotong University. The grant from 'Long Yuan Qing Nian' of Gansu Province also is acknowledged.

Appendix A. Supplementary material

Crystallographic data (excluding structure factors) for the structures reported in this paper have been deposited with the Cambridge Crystallographic Data Centre with reference number CCDC 872018. Copies of the data can be obtained, free of charge, on application to the CCDC, 12 Union Road, Cambridge CB2 1EZ, UK. Tel: +44-01223-762910; fax: +44-01223-336033; e-mail: deposit@ccdc.cam.ac.uk or http://www.ccdc.cam.ac.uk. Supplementary data associated with this article can be found, in the online version, at http://dx.doi.org/10.1016/j.jphotobiol.2012.07.005.

References

[1] Reedijk J, Comprehensive Coordination Chemistry, vol. 2, Pergamon, Oxford, 1987 (Chapter 13.2).
[2] S.X. Wang, S.Y. Yu, Q.H. Luo, Synthesis, structure and electrochemical behaviour of cobalt(II) complexes with 2,6-bis(benzimidazol-2′-yl) pyridine, Transition. Met. Chem. 19 (1994) 205–208.
[3] J.B. Wright, The chemistry of the benzimidazoles, Chem. Rev. 48 (1951) 397–541.
[4] N.T.A. Ghani, A.M. Mansour, Novel Pd(II) and Pt(II) complexes of N, N-donor benzimidazole ligand: synthesis, spectral, electrochemical, DFT studies and evaluation of biological activity, Inorg. Chim. Acta. 373 (2011) 249–258.
[5] J. Mann, A. Baron, Y. Opoku-Boahen, E. Johansson, G. Parkinson, L.R. Kelland, S. Neidle, A new class of symmetric bis-benzimidazole-based DNA minor groove binding agents, J. Med. Chem. 44 (2001) 138–144.
[6] J.Y. Xu, Y. Zeng, Q. Ran, Z. Wei, Y. Bi, Q.H. He, Q.J. Wang, S. Hu, J. Zhang, M.Y. Tang, W.Y. Hua, X.M. Wu, Synthesis and biological activity of 2-alkylbenzimidazoles bearing a *N*-phenylpyrrole moiety as novel angiotensin II AT1 receptor antagonists, Bioorg. Med. Chem. Lett. 17 (2007) 2921–2926.
[7] P.D. Patel, M.R. Patel, N. Kaushik-Basu, T.T. Talele, 3D QSAR and molecular docking studies of benzimidazole derivatives as hepatitis C virus NS5B polymerase Inhibitors, J. Chem. Inf. Model. 48 (2008) 42–55.
[8] E.E. Alberto, L.L. Rossato, S.H. Alves, D. Alves, A.L. Braga, Imidazolium ionic liquids containing selenium: synthesis and antimicrobial activity, Org. Biomol. Chem. 9 (2011) 1001–1003.
[9] S. Estrada-Soto, R. Villalobos-Molina, F. Aguirre-Crespo, J. Vergara-Galicia, H. Oreno-DÍaz, M. Torres-Piedra, G. Navarrete-Vázquez, Relaxant activity of 2-(substituted phenyl)-1H-benzimidazoles on isolated rat aortic rings: design and synthesis of 5-nitro derivatives, Life. Sci. 79 (2006) 430–435.
[10] V. Rajendiran, M. Murali, E. Suresh, S. Sinha, K. Somasundaram, M. Palaniandavar, Mixed ligand ruthenium(II) complexes of bis(pyrid-2-yl)-/bis(benzimidazol-2-yl)-dithioether and diimines: study of non-covalent DNA binding and cytotoxicity, Dalton. Trans. 2008 (2008) 148–163.
[11] H.Y. Liu, H. Wu, J. Yang, Y.Y. Liu, B. Liu, Y.Y. Liu, J.F. Ma, PH-Dependent assembly of 1D to 3D octamolybdate hybrid materials based on a new flexible bis-[(pyridyl)-benzimidazole] ligand, Cryst. Growth. Des. 11 (2011) 2920–2927.
[12] Y.M. Song, Q. Wu, P.J. Yang, N.N. Luan, L.F. Wang, Y.M. Liu, DNA binding and cleavage activity of Ni(II) complex with all-trans retinoic acid, J. Inorg. Biochem. 100 (2006) 1685–1691.
[13] J. Tan, B. Wang, L. Zhu, DNA binding, cytotoxicity, apoptotic inducing activity, and molecular modeling study of quercetin zinc(II) complex, Bioorg. Med. Chem. 17 (2009) 614–620.
[14] C.P. Tan, J. Liu, L.M. Chen, S. Shi, L.N. Ji, Synthesis, structural characteristics, DNA binding properties and cytotoxicity studies of a series of Ru(III) complexes, J. Inorg. Biochem. 102 (2008) 1644–1653.
[15] L.Z. Zhang, G.Q. Tang, The binding properties of photosensitizer methylene blue to herring sperm DNA: a spectroscopic study, J. Photochem. Photobiol. B. 74 (2004) 119–125.
[16] L.N. Ji, X.H. Zou, J.G. Lin, Shape- and enantioselective interaction of Ru(II)/Co(III) polypyridyl complexes with DNA, Coord. Chem. Rev. 216–217 (2001) 513–536.
[17] B.M. Zeglis, V.C. Pierre, J.K. Barton, Metallo-intercalators and metallo-insertors, Chem. Commun. 44 (2007) 4565–4579.
[18] S. Gopal, U.N. Balachandran, Synthesis, characterization and DNA binding studies of new ruthenium(II) bisterpyridine complexes, Eur. J. Med. Chem. 45 (2010) 284–291.
[19] J.J. Perry IV, J.A. Perman, M.J. Zaworotko, Design and synthesis of metal–organic frameworks using metal–organic polyhedra as supermolecular building blocks, Chem. Soc. Rev. 38 (2009) 1400–1417.
[20] J.P. Zhang, X.C. Huang, X.M. Chen, Supramolecular isomerism in coordination polymers, Chem. Soc. Rev. 38 (2009) 2385–2396.
[21] M.G. Moeller, L.F. Campo, A. Brandelli, V. Stefani, Synthesis and spectroscopic characterisation of 2-(2-hydroxyphenyl)benzazole isothiocyanates as new fluorescent probes for proteins, J. Photochem. Photobiol. A. 149 (2002) 217–225.
[22] J.M. Grevy, F. Tellez, S. Bernés, H. Nöth, R. Contreras, N. Barba-Behrens, Coordination compounds of thiabendazole with main group and transition metal ions, Inorg. Chim. Acta. 339 (2002) 532–542.

[23] H.L. Wu, X.C. Huang, J.K. Yuan, F. Kou, F. Jia, B. Liu, K.T. Wang, A V-shaped ligand 2,6-bis(2-benzimidazolyl)pyridine and its picrate Mn(II) complex: synthesis, crystal structure and DNA-binding properties, Eur. J. Med. Chem. 45 (2010) 5324–5330.
[24] H.L. Wu, K.T. Wang, B. Liu, F. Kou, F. Jia, J.K. Yuan, Y. Bai, Synthesis, characterization, crystal structure and DNA-binding studies of two zinc(II) complexes with the V-shaped bis(benzimidazole)-thiapropane and its derivative ligand, Inorg. Chim. Acta 384 (2012) 302–308.
[25] H.L. Wu, J.K. Yuan, Y. Bai, G.L. Pan, H. Wang, X.B. Shu, Synthesis, structure, DNA-binding properties and antioxidant activity of a nickel(II) complex with bis(*N*-allylbenzimidazol-2-ylmethyl)benzylamine, J. Photochem. Photobiol. B. 107 (2012) 65–72.
[26] H.L. Wu, J.K. Yuan, Y. Bai, F. Jia, B. Liu, F. Kou, J. Kong, Synthesis, structure, DNA-binding properties, and antioxidant activity of copper(II) and cobalt(II) complexes with bis(*N*-allylbenzimidazol-2-ylmethyl)benzylamine, Transition. Met. Chem. 36 (2011) 819–827.
[27] S. Satyanarayana, J.C. Dabrowiak, J.B. Chaires, Tris(phenanthroline)ruthenium(II) enantiomer interactions with DNA: mode and specificity of binding, Biochemistry 32 (1993) 2573–2584.
[28] M.E. Reichmann, S.A. Rice, C.A. Thomas, P. Doty, A further examination of the molecular weight and size of desoxypentose nucleic acid, J. Am. Chem. Soc. 76 (1954) 3047–3051.
[29] K. Takahashi, Y. Nishida, S. Kida, Crystal structure of copper(II) complex with N, N-bis(2-benzimidazolylmethyl)benzylamine, Polyhedron 3 (1984) 113–116.
[30] Bruker, Smart Saint and Sadabs, Bruker Axs, Inc., Madison, WI, 2000.
[31] G.M. Sheldrick, SHELXTL, Siemens Analytical X-ray Instruments, Inc., Madison, Wisconsin, USA, 1996.
[32] R. Gaur, R.A. Khan, S. Tabassum, P. Shah, M.I. Siddiqi, L. Mishra, Interaction of a ruthenium(II)–chalcone complex with double stranded DNA: spectroscopic, molecular docking and nuclease properties, J. Photochem. Photobiol. A. 220 (2011) 145–152.
[33] A.M. Pyle, J.P. Rehmann, R. Meshoyrer, C.V. Kumar, N.J. Turro, J.K. Barton, Mixed-ligand complexes of ruthenium(II): factors governing binding to DNA, J. Am. Chem. Soc. 111 (1989) 3051–3058.
[34] A. Wolf, G.H. Shimer, T. Meehan, Polycyclic aromatic hydrocarbons physically intercalate into duplex regions of denatured DNA, Biochemistry 26 (1987) 6392–6396.
[35] B.C. Baguley, M.L. Bret, Quenching of DNA-ethidium fluorescence by amsacrine and other antitumor agents: a possible electron-transfer effect, Biochemistry 23 (1984) 937–943.
[36] J.R. Lakowicz, G. Webber, Quenching of fluorescence by oxygen probe for structural fluctuations in macromolecules, Biochemistry 12 (1973) 4161–4170.
[37] C.C. Winterbourn, Hydroxyl radical production in body fluids. Roles of metal ions, ascorbate and superoxide, Biochem. J. 198 (1981) 125–131.
[38] C.C. Winterbourn, Comparison of superoxide with other reducing agents in the biological production of hydroxyl radicals, Biochem. J. 182 (1979) 625–628.
[39] Z.Y. Guo, R.E. Xing, S. Liu, H.H. Yu, P.B. Wang, C.P. Li, P.C. Li, The synthesis and antioxidant activity of the Schiff bases of chitosan and carboxymethyl chitosan, Bioorg. Med. Chem. Lett. 15 (2005) 4600–4603.
[40] C. Beauchamp, I. Fridovich, Superoxide dismutase: improved assays and an assay applicable to acrylamide gels, Anal. Biochem. 44 (1971) 276–287.
[41] Q.H. Luo, Q. Lu, A.B. Dai, L.G. Huang, A study on the structure and properties of a new model compound of Cu(II) Zn(II)-superoxide dismutase, J. Inorg. Biochem. 51 (1993) 655–662.
[42] W.K. Dong, C.Y. Zhao, Y.X. Sun, X.L. Tang, X.N. He, Synthesis and structure of an unprecedented supramolecular bridged-hydroxyl manganese(III)-lithium(I) coordination polymer [Mn(III)L(OH)(2)Li(I)](n) through both intermolecular hydrogen bonds and π–π stacking interactions, Inorg. Chem. Commun. 12 (2009) 234–236.
[43] W.J. Geary, The use of conductivity measurements in organic solvents for the characterization of coordination compounds, Coord. Chem. Rev. 7 (1971) 81–122.
[44] C.Y. Su, B.S. Kang, C.X. Du, Q.C. Yang, T.C. Mak, Formation of mono-, bi-, tri-, and tetranuclear Ag(I) complexes of C_3-symmetric tripodal benzimidazole ligands, Inorg. Chem. 39 (2000) 4843–4849.
[45] T.J. Lane, I. Nakagawa, J.L. Walter, A.J. Kandathil, Infrared investigation of certain imidazole derivatives and their metal chelates, Inorg. Chem. 1 (1962) 267–276.
[46] E.K. Chec, M. Kubiak, T. Glowiak, J.J. Ziolkowski, Synthesis, crystal and molecular structure of the novel complex [dinitrato{N, N-bis(1–methylbenzimidazol-2–ylmethyl)methylamine}]cobalt(II), Transition. Met. Chem. 23 (1998) 641–644.
[47] M. McKee, M. Zvagulis, C.A. Reed, Further insight into magnetostructural correlations in binuclear copper(II) species related to methemocyanin: x-ray crystal structure of 1,2-.mu.-nitrito complex, Inorg. Chem. 24 (1985) 2914–2919.
[48] K. Nakamoto (Ed.), Infrared and Raman Spectra of Inorganic and Coordination Compounds, Wiley, New York, 1978, p. 305.
[49] J.H.S.K. Monteiro, R.D. Adati, M.R. Davolos, J.R.M. Vicenti, R.A. Burrow, Correlation between structural data and spectroscopic studies of a new β-diketonate complex with trivalent europium and gadoliniumwz, New. J. Chem. 35 (2011) 1234–1241.
[50] K.N. Power, T.L. Hennigar, M.J. Zaworotko, Crystal structure of the coordination polymer [Co(bipy)1.5(NO3)2]CS2 (bipy=4,4-bipyridine), a new motif for a network sustained by T-shape building blocks, New. J. Chem. 22 (1998) 177–181.
[51] Q.Y. Yang, S.R. Zheng, R. Yang, M. Pan, R. Cao, C.Y. Su, An unusual 3D coordination polymer assembled through parallel interpenetrating and polycatenating of (6,3) nets, Cryst. Eng. Commun. 11 (2009) 680–685.
[52] C.L. Chen, C.Y. Su, Y.P. Cai, H.X. Zhang, A.W. Xu, B.S. Kang, Z.L. Hans-Conrad, Multidimensional frameworks assembled from silver(I) coordination polymers containing flexible bis(thioquinolyl) ligands: role of the intra- and intermolecular aromatic stacking interactions, Inorg. Chem. 42 (2003) 3738–3750.
[53] W.K. Dong, Y.X. Sun, C.Y. Zhao, X.Y. Dong, L. Xu, Synthesis, structure and properties of supramolecular Mn(II), Co(II), Ni(II) and Zn(II) complexes containing Salen-type bisoxime ligands, Polyhedron 29 (2010) 2087–2097.
[54] S. Satyanarayana, J.C. Dabroniak, J.B. Chaires, Neither.DELTA.- nor.LAMBDA.-tris(phenanthroline)ruthenium(II) binds to DNA by classical intercalation, Biochemistry 31 (1992) 9319–9324.
[55] D. Suh, J.B. Chaires, Criteria for the mode of binding of DNA binding agents, Bioorg. Med. Chem. 3 (1995) 723–728.
[56] R. Palchaudhuri, P.J. Hergenrother, DNA as a target for anticancer compounds: methods to determine the mode of binding and the mechanism of action, Curr. Opin. Biotechnol. 18 (2007) 497–503.
[57] B.D. Wang, Z.Y. Yang, P. Crewdson, D.Q. Wang, Synthesis, crystal structure and DNA-binding studies of the Ln(III) complex with 6-hydroxychromone-3-carbaldehyde benzoyl hydrazine, J. Inorg. Biochem. 101 (2007) 1492–1504.
[58] V.K. Verma, A.K. Asatkar, T.A. Jain, S.K. Tripathi, R. Singh, P.B. Hitchcock, S. Nigam, S.K. Gupta, Synthesis, structure and DNA binding studies of mononuclear copper(II) complexes with mixed donor macroacyclic ligands, 2,6-bis({*N*-[2&3-(phenylselenato)alkyl]}benzimidoyl)-4-methylphenol, Polyhedron 28 (2009) 2591–2598.
[59] J. Liu, T.X. Zhang, L.N. Ji, DNA-binding and cleavage studies of macrocyclic copper(II) complexes, J. Inorg. Biochem. 91 (2002) 269–276.
[60] H. Xu, K.C. Zheng, Y. Chen, Y.Z. Li, L.J. Lin, H. Li, P.X. Zhang, L.N. Ji, Dalton. Trans. 2003 (2003) 2260–2268.
[61] S. Nafisi, A.A. Saboury, N. Keramat, J.F. Neault, H.A. Tajmir-Riahi, Stability and structural features of DNA intercalation with ethidium bromide, acridine orange and methylene blue, J. Mol. Struct. 827 (2007) 35–43.
[62] G.W. Zhang, X. Hu, P. Fu, Spectroscopic studies on the interaction between carbaryl and calf thymus DNA with the use of ethidium bromide as a fluorescence probe, J. Photochem. Photobiol. B. 108 (2012) 53–61.
[63] J. Liu, T. Zhang, T. Lu, L. Qu, H. Zhou, Q. Zhang, L. Ji, DNA-binding and cleavage studies of macrocyclic copper(II) complexes, J. Inorg. Biochem. 91 (2002) 269–276.
[64] Y.B. Zeng, N. Yang, W.S. Liu, N. Tang, Synthesis, characterization and DNA-binding properties of La(III) complex of chrysin, J. Inorg. Biochem. 97 (2003) 258–264.
[65] C.V. Kumar, J.K. Barton, N.J. Turro, Photophysics of ruthenium complexes bound to double helical DNA, J. Am. Chem. Soc. 107 (1985) 5518–5523.
[66] T. Ihara, S. Sueda, A. Inenaga, R. Fukuda, M. Takagi, Synthetic DNA ligands conjugated with metal binding moiety. Regulation of the interaction with DNA by metal ions and the ligand effect on metal assisted DNA cleaving, Supramol. Chem. 8 (1997) 93–111.
[67] S. Yellappa, J. Seetharamappa, L.M. Rogers, R. Chitta, R.P. Singhal, F. D'Souza, Binding, electrochemical activation, and cleavage of DNA by cobalt(II)tetrakis-*N*-methylpyridyl porphyrin and its *b*-pyrrole brominated derivative, Bioconjugate. Chem. 17 (2006) 1418–1425.
[68] M. Shakir, M. Azam, M.F. Ullah, S.M. Hadi, Synthesis, spectroscopic and electrochemical studies of N, N-bis[(E)-2-thienylmethylidene]-1,8-naphthalene–diamine and its Cu(II) complex: DNA cleavage and generation of superoxide anion, J. Photochem. Photobiol. B. 104 (2011) 449–456.
[69] S.B. Bukhari, S. Memon, M. Mahroof-Tahir, M.I. Bhanger, Synthesis, characterization and antioxidant activity copper–quercetin complex, Spectrochim. Acta. A. Mol. Biomol. Spectrosc. 71 (2009) 1901–1906.
[70] F.V. Botelho, J.I. Alvarez-Leite, V.S. Lemos, A.M.C. Pimenta, H.D.R. Calado, T. Matencio, C.T. Miranda, E.C. Pereira-Maia, Physicochemical study of floranol, its copper(II) and iron(III) complexes, and their inhibitory effect on LDL oxidation, J. Inorg. Biochem. 101 (2007) 935–943.
[71] Q. Wang, Z.Y. Yang, G.F. Qi, D.D. Qin, Synthesis, crystal structure, antioxidant activities and DNA-binding studies of the Ln(III) complexes with 7-methoxychromone-3-carbaldehyde-(4-hydroxy) benzoyl hydrazone, Eur. J. Med. Chem. 44 (2009) 2425–2433.
[72] T.R. Li, Z.Y. Yang, B.D. Wang, D.D. Qin, Synthesis, characterization, antioxidant activity and DNA-binding studies of two rare earth(III) complexes with naringenin-2-hydroxy benzoyl hydrazone ligand, Eur. J. Med. Chem. 43 (2008) 1688–1695.
[73] J.I. Ueda, N. Saito, Y. Shimazu, T. Ozawa, A comparison of scavenging abilities of antioxidants against hydroxyl radicals, Arch. Biochem. Biophys. 333 (1996) 377–384.